

Establishing Reproducibility and Correlation of Cochlear Microphonic Amplitude to Implant Electrode Position Using Intraoperative Electrocochleography and Postoperative Cone Beam Computed Tomography

Andrew Soulby,¹ Steve Connor,^{2,3} Dan Jiang,^{1,5} Terry Nunn,¹ Patrick Boyle,⁴ and Irumee Pai^{1,3}

Objectives: The primary objective of this study was to establish the reproducibility of cochlear microphonic (CM) recordings obtained from a cochlear implant (CI) electrode contact during and immediately after insertion. This was achieved by evaluating the insertion angle and calculating the position of the apical electrode contact during insertion, using postoperative cone beam computed tomography (CBCT). The secondary objective was to create individualized patient maps of electrode contacts located within acoustically sensitive regions by correlating the CM amplitude to the electrode position determined using CBCT.

Methods: CMs were recorded from a CI electrode contact during and immediately after insertion in 12 patients ($n=14$ ears). Intraoperative recordings were made for a 0.5kHz tone burst stimulus and were recorded from the apical electrode contact. Postinsertion recordings were made from the odd-numbered electrode contacts (1–15) along the array, using a range of stimulus frequencies (from 0.125 to 2kHz). The time point at which each electrode contact passed through the round window was noted throughout the insertion, and the CM amplitude at this point was correlated to postoperative CBCT. This correlation was then used to estimate the CM amplitude at particular points within the cochlea, which was in turn compared with the amplitudes recorded from each electrode postoperatively to assess the reproducibility of the recordings.

Results: Significant correlation was shown between intraoperative insertion and postinsertion angles at two amplitude events (maximum amplitude: 29° mean absolute error, $r=0.77$, $p=0.006$; 10% of maximum amplitude: 52° mean absolute error, $r=0.85$, $p=0.002$).

Conclusion: We have developed a novel method to demonstrate the reproducibility of the CM responses recorded from a CI electrode during insertion. By correlating the CM amplitude with the postoperative CBCT, we have also been able to create individualized maps of CM responses, categorizing the cochlea into acoustically responsive and unresponsive regions. If the electrode contacts within the acoustically sensitive regions are shown to be associated with improved loudness discrimination, it could have implications for optimal electrode mapping and placement.

Key words: Cochlear Implant, Cochlear Microphonic, Cone Beam CT, Electrocochleography.

Abbreviations: ECochG = Electrocochleography; CM = Cochlear Microphonic; SP = Summating Potential; ANN = Auditory Nerve Neurophonic; CAP = Compound Action Potential; CI = Cochlear Implant; CBCT = Cone Beam Computer Tomography; P_{ATH} = Predicted audiometric threshold from ECochG; DF = Degrees of Freedom; AB = Advanced Bionics; NICE = National Institute for Health and Care Excellence; PTA = Pure Tone Audiometry; SD = Standard Deviation.

(Ear & Hearing 2021;42;1263–1275)

INTRODUCTION

Electrocochleography

Electrocochleography (ECochG) is the measurement of electrical potentials generated by the cochlea in response to an auditory stimulus. There are four parts to the classical ECochG response: cochlear microphonic (CM), summating potential, auditory nerve neurophonic (ANN), and compound action potential (Snyder and Schreiner 1984; Henry 1995; Choudhury et al. 2012; Eggermont 2019).

ECochG can inform us of the combined function of outer and inner hair cells along with their tonotopic location and the successful transduction of their movements into neural impulses. Perhaps the best-known examples of clinical utilization of ECochG are the evaluation of the summating potential/AP ratio in Meniere's disease (Conlon and Gibson 2000) and the measurement of CM portion of the ECochG response for determination of the sensory or neural nature of a hearing loss (Santarelli and Arslan 2002).

Electrocochleography and Cochlear Implants

The changes in electrical potential responsible for the CM response are detectable “far-field” beyond the tonotopic location of the stimulating frequency due to volume conduction, which combines the effects of tissue conductivity, dipole direction, and spatial distance. As the recording electrode approaches the main site of the CM generation, it becomes “near-field” and these effects diminish significantly, resulting in an increase in signal amplitude (Rutkove 2007). Because of this, although cochlear implant (CI) recipients have far poorer hair cell function than individuals with normal hearing, the recorded response from a CI in situ is often orders of magnitude larger than from the mastoid or round window (RW) promontory (Dalbert et al. 2015). This means that, if present, the signal requires little averaging to resolve from the noise, even though a speech processor has a higher noise floor than a dedicated electrophysiology machine. Thus, the CM can

¹St. Thomas' Hearing Implant Centre, Guy's and St. Thomas' NHS Foundation Trust, London, United Kingdom; ²Department of Radiology, Guy's and St. Thomas' NHS Foundation Trust, London, United Kingdom; ³School of Biomedical Engineering & Imaging Sciences Clinical Academic Group, King's College London, London, United Kingdom; ⁴Advanced Bionics GmbH, European Research Centre, Hannover, Germany; and ⁵Centre for Craniofacial and Regenerative Biology, King's College London, London, United Kingdom.

Supplemental digital content is available for this article. Direct URL citations appear in the printed text and are provided in the HTML and text of this article on the journal's Web site (www.ear-hearing.com).

Copyright © 2021 The Authors. Ear & Hearing is published on behalf of the American Auditory Society, by Wolters Kluwer Health, Inc. This is an open-access article distributed under the terms of the Creative Commons Attribution-Non Commercial-No Derivatives License 4.0 (CCBY-NC-ND), where it is permissible to download and share the work provided it is properly cited. The work cannot be changed in any way or used commercially without permission from the journal.

be gathered quickly, easily, reproducibly, and in real time (Harris et al. 2017). The ability to record CMs from in situ CI electrodes in humans was piloted relatively recently (Campbell et al. 2016) and has been developed over the last few years.

Although the great majority of CI recipients have compromised hair cell function (Rance et al. 1999), measuring CMs in these patients may still provide useful information. It has been demonstrated in a number of studies that the CM is related to measurable hearing at the stimulus frequency used, or, more generally, to speech perception derived from the residual cochlear function (Laureano et al. 1995; Santarelli et al. 2006; Fitzpatrick et al. 2014; Koka et al. 2017). It is therefore plausible that monitoring the CM could provide information on cochlear function in real time (Campbell et al. 2016).

One potential use for this is during electrode insertion in CI surgery; several groups (Harris et al. 2017; Bester et al. 2017), including our center, are currently investigating the use of the CM amplitude as a form of intraoperative feedback during electrode insertion to improve hearing preservation rates. A second use for measuring CMs is their ability to predict hearing thresholds due to correlation with cochlear function (Koka et al. 2017). If the frequency-specific CM responses prove to correlate well with pure tone audiometry (PTA) thresholds, they could then be utilized for CI mapping in electroacoustic stimulation (EAS) cases.

Finally, it is likely, from what we understand of the interdependency of the hearing pathway, that the preservation of hair cells in particular regions of the cochlea is related to preservation of other cell types such as supporting and neuronal populations (Terayama et al. 1977; Webster and Webster 1981; Nayagam et al. 2011). Therefore, if the hearing pathway is intact at a particular frequency, for example, when there is a clearly measurable pure tone threshold and a detectable CM in a patient who has historically been well aided, then it is possible that spiral ganglion neuronal preservation would also be greater in these regions (Leake et al. 1999; Dodson and Mohuiddin 2000; O'Neil et al. 2011). There is evidence that neuronal preservation does influence CI outcome (Eppsteiner et al. 2012; Seyyedi et al. 2014; Tropitzch et al. 2019). Thus, if it were possible to know which regions of the cochlea still contained enough hair cells to generate a CM, it might be possible to use this information to individualize and optimize mapping for electrode contacts falling within this region.

The first step in assessing this would be to confidently establish the reproducibility of CMs generated intraoperatively and to be able to ascertain where the apical recording electrode is located in the cochlea at any point in time during the insertion. In this article, we describe a novel method to establish the reliability of intraoperative CM recordings and to correlate them to specific locations within individual cochleae, using postoperative cone beam computed tomography (CBCT).

MATERIALS AND METHODS

A longitudinal observational feasibility study was carried out at St. Thomas' Hearing Implant Centre, London, United Kingdom. Approvals were obtained from the South East Coast Surrey NHS Research Ethics Committee (IRAS: 214480). Guy's and St. Thomas' research and development department acted as study sponsors. The study is registered on the clinicaltrials.gov website (NCT03848338).

Inclusion Criteria

Participants were recruited from patients who were due to undergo cochlear implantation with one or more Advanced Bionics (AB) CIs at St. Thomas' Hearing Implant Centre, London, United Kingdom. The inclusion criteria were as follows:

- Eligible for CI according to the National Institute for Health and Care Excellence (NICE) guidelines
- Recordable hearing at 0.5 kHz on PTA, preferably ≤ 80 dB HL
- Normal cochleae and cochlear nerves on preoperative MRI
- Able to provide fully informed consent for study participation
- No contraindications to following a routine clinical rehabilitation plan

Equipment

Audiometry was carried out using calibrated Astera audiometers and TDH-39 headphones. ECoChG measurements were made using either the AB "Black Box 2" device or the AB "Active Insertion Monitoring (AIM) Tablet." Both used a CPI3 programming module to connect to a Naida Q90 speech processor and UHP 3D headpiece with a maximum strength magnet to receive and process the ECoChG signal. To generate the auditory stimuli, both devices used a Behringer USB Soundcard connected to an Etymotics 3A insert, which generated tone bursts of up to 110 dB SPL at half-octaves from 0.125 to 4 kHz. This output was checked using a 2 cc coupler (See Figure in Supplemental Digital Content 2, <http://links.lww.com/EANDH/A772>), but no calibration of these signals was performed on a patient by patient basis.

Surgical Protocol

Before surgery, the ear to be implanted was cleared of wax and washed out with Povidone-iodine or chlorohexidine before an Etymotics 3A tip was inserted. Once it was securely positioned, the pinna was carefully folded forward and secured with

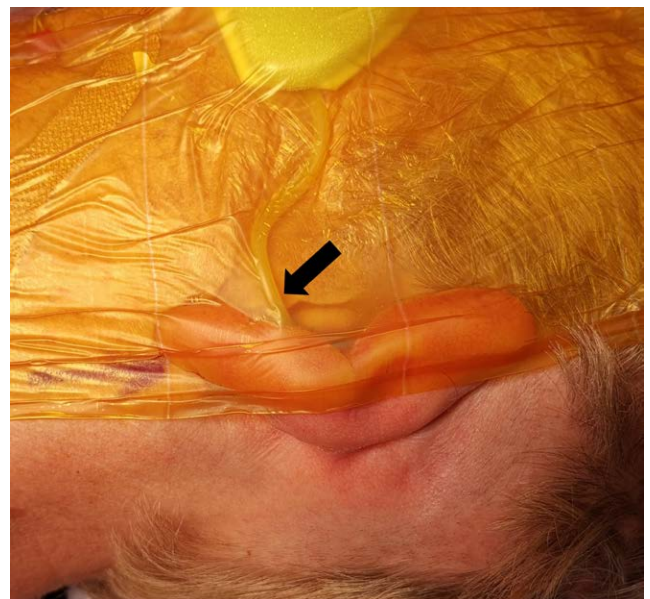


Fig. 1. Securing the earphone insert before placement of the surgical drapes, the black arrow denotes the acoustic tube coming from the in situ ear insert.

Ioban drape (3M), and skin preparation and draping of the surgical site were completed in a standard manner (Fig. 1).

All surgeries were performed using a transmastoid/posterior tympanotomy approach, “soft surgery” techniques and RW electrode array insertion. Once the receiver-stimulator package was secured within a periosteal pocket over a bony recess, the external processor covered in a sterile sleeve was electromagnetically coupled to the internal device through the surgical drapes.

A slow insertion of the electrode array was performed for every case (approximately 3 min), with the operating surgeon calling out as each electrode contact passed through the RW. These points were noted on the CM trace, such that the distance of the apical electrode contact inside the cochlea could be correlated with time and thus CM amplitude (Fig. 2). No audible or any other feedback on the ECochG signal was provided to the surgeon during the insertion so as not to influence the surgical behavior, and the standard practice of aiming for full insertion wherever possible was observed.

Postoperative Protocol

All patients received at least one dose of intravenous dexamethasone intraoperatively (standard dose 6.6 mg in adult cases), but there was a marked variability in the steroid therapy regime otherwise, including direct application to the RW membrane, 1–2 further doses of intravenous dexamethasone and 3-day course of oral prednisolone (30 mg once daily).

CBCT was performed in all those who tolerated the procedure, usually within 24 hours of surgery and always before device activation (around 4 weeks after surgery). ECochG and PTA were performed twice within the first 3 months, typically at switch-on or at week 1 postactivation, and then at 6 weeks or 3 months postactivation. The ECochG measurements made at these follow-up appointments after device activation are referred to as “postoperative recordings” in the rest of this article.

Electrocochleography Measurements

CM measurements during electrode array insertion (referred to as “intraoperative recordings”) were recorded using 50 ms duration 110 dB SPL 0.5 kHz acoustic stimuli, including 5 ms onset and offset ramps. Presentations were paired such that the phase of successive stimuli was inverted (rarefaction and condensation). Response recording was synchronized to stimulus delivery to maintain the known phase relationship. The recorded signal was converted into a 9-bit (8 plus sign) digital signal in the implant before being wirelessly transmitted using the back-telemetry pathway used to record impedances and electrically evoked compound action potentials. For a 500 Hz stimulus, approximately 8 complete positive and negative stimulus pairs were delivered per second with the full waveform being recorded to a javascript object notation file format.

To determine the CM signal, successive stimuli recordings of the opposing phase were subtracted from each other. A fast-Fourier transform was then applied to convert the signal from the

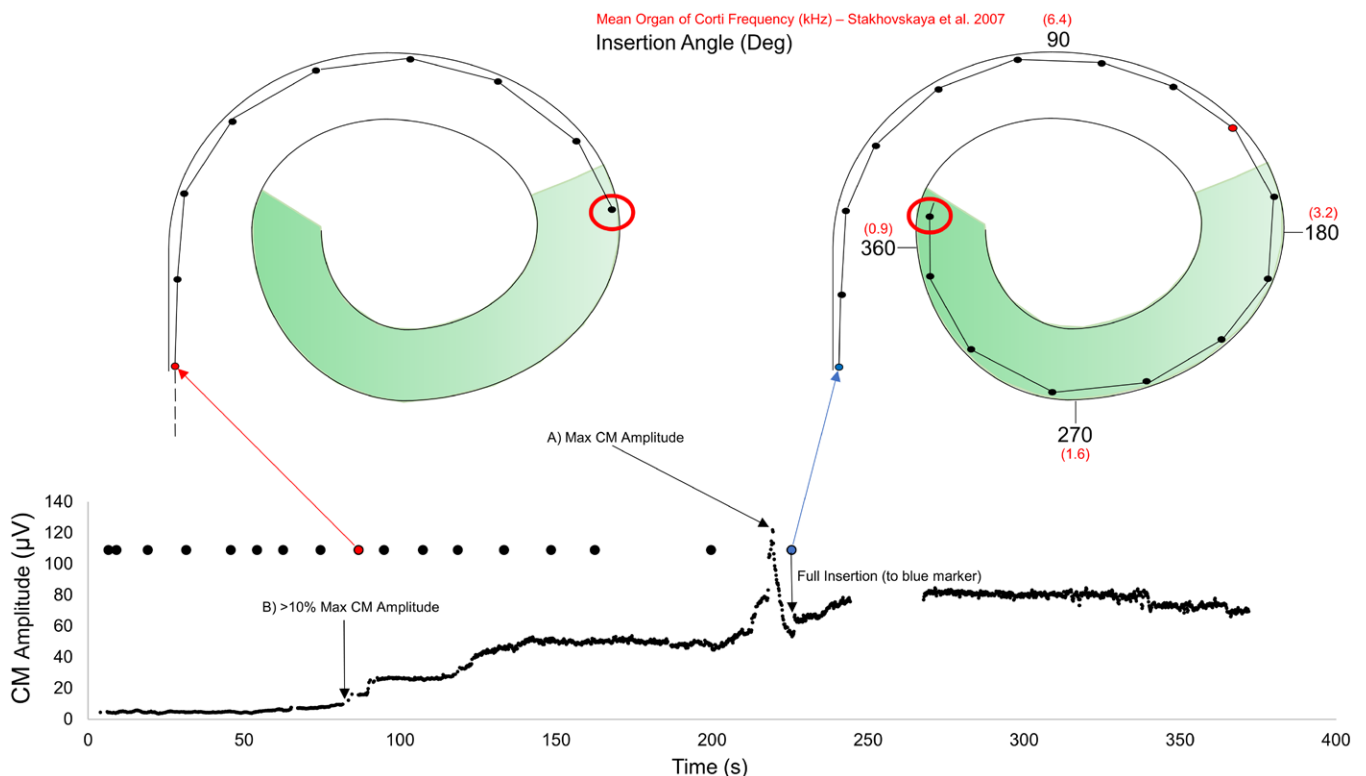


Fig. 2. Example cochlear microphonic amplitude trace during array insertion, including notation of electrodes as they enter the round window (black dots). Illustrated above are (left) estimation of apical electrode position during insertion and (right) determination of electrodes whose final position is within the cochlear microphonic responsive region (green). Also noted on this trace are events (A) the max CM amplitude and (B) when the CM >10% of max amplitude, which were used for CBCT correlation analysis. CBCT indicates cone beam computed tomography; CM, cochlear microphonic.

time to the frequency domain, and the amplitude at the stimulus frequency was plotted over time to create the intraoperative trace. The noise floor of the signal was estimated using the mean of a range of frequency bins adjacent to the stimulus frequency bin. Of note, when the term “CM” is used in this article, we thus refer to the microphonic or difference (CM/DIF) amplitude recorded at the fundamental stimulus frequency. It should also be borne in mind that, while the measurement recorded is dominated by part of the CM, the ANN when present will also contribute to, or subtract from, the recorded signal depending on phase.

During the intraoperative recording, the software was configured to average recordings up to a maximum of 40 repetitions or until a signal-to-noise ratio of 24 dB was achieved. An SNR of 3:1 was taken as the limit of detection for a valid CM.

Once insertion was complete and the implant cable coiled securely within the mastoid cavity, a battery of further recordings were made (referred to as “postinsertion” recordings), which consisted of electrode sweeps (recording for one stimulus frequency from each odd-numbered electrode contact) and a frequency sweep (recording from the apical electrode contact across all audiometric frequencies) to generate a predicted audiogram. The formula used by the software to generate the predicted hearing threshold (P_{ATH}) was:

$$P_{ATH} = S - 20 \times \log_{10}\left(\frac{C}{0.25}\right)$$

where *S* is the stimulus level in dB SPL and *C* is the CM amplitude. The software used a single stimulus level from which to plot a linear regression. The stimulus frequencies used were between 0.125 and 2 kHz at semi-octave intervals. All postinsertion measurements used the same stimulus set-up and intensity (110 dB SPL).

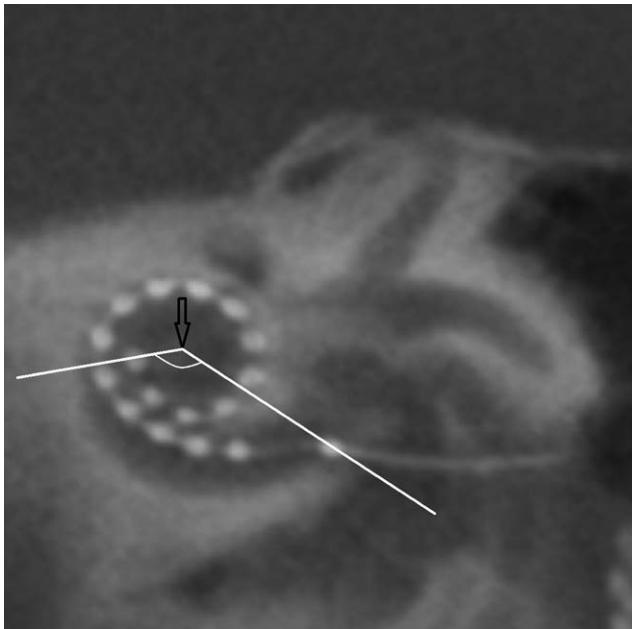


Fig. 3. Double oblique coronal reformatted image through the basal turn with a 2 mm average slab reconstruction designed to demonstrate the entire electrode array. The open black arrow indicates the mid-modiolar point and the angle is shown between the round window (where the reference electrode is located) and the distal electrode contact (added to 360° to calculate the electrode array angular insertion).

The exact ECochG testing regime evolved throughout the pilot as we acquired an understanding of which measurements would be most useful at which times.

Cone Beam CT Analysis

Every CBCT scan was analyzed by a neuroradiologist of 19 years' consultant experience. The final insertion angle of the apical electrode contact was estimated to the nearest 5° (Fig. 3) and scala tympani retention assessed over the length of the array, as per the standard practice at our center (Fig. 4A, B).

For intraoperative measurements (i.e., during electrode array insertion), the position of the apical electrode contact, expressed as angular insertion from the RW, was calculated to the nearest degree for selected CM event markers at 0.5 kHz, namely the peak amplitude (A) and when the CM exceeded 10% of the peak amplitude (B). However, we acknowledge that the precision of this measurement is likely to be in the order of 10°. To make this calculation, the distance between the apical electrode contact and the electrode contact passing through the RW at the time of the CM event was determined from the known electrode array dimensions and spacing between electrode contacts (Table 2). This distance was then superimposed on the CBCT of the final electrode array position and the presumed angular insertion of the apical electrode contact at the time of the CM event was calculated from the RW (Fig. 5).

For postinsertion measurements, the final insertion angle of the electrode contacts corresponding to the 2 CM event markers A and B (A=peak amplitude and B=>10% peak amplitude) were calculated to the nearest 10° for each frequency (0.125–2 kHz) where a clear response was recorded.

Hearing Preservation Analysis

The hearing preservation rates were determined at device activation, using the Skarzynski formula (Skarzynski et al. 2013). Comparison between actual hearing preservation and the preservation predicted by the intraoperative CM traces was based on the A, B, and C trace classification system described by Harris et al. 2017 (A: increasing and maintained CM=suggested hearing preservation, B: initially increasing and then a decrease in CM and C: CM fluctuating throughout=loss of residual hearing). This classification system was modified by permitting traces where there was a moderate (<50%) drop in CM amplitude toward the end of the insertion to be included into the A category, similarly to the type 2 and type 3 traces described in Koka et al. (2018).

Statistical Analysis

Descriptive statistics were used for demographic, hearing preservation, and PTA vs. ECochG threshold data. For the insertion angle correlation analysis, a Pearson correlation coefficient (*r*) was calculated using the absolute error in degrees between the intraoperative and postinsertion variables of both the max CM amplitude and >10% max CM amplitude points, which indicates strength of the association between these two variables (with 0 being no correlation, and 1 or –1 being perfect positive or negative correlation, respectively). Since the *r* value itself does not indicate the significance of a correlation, this was

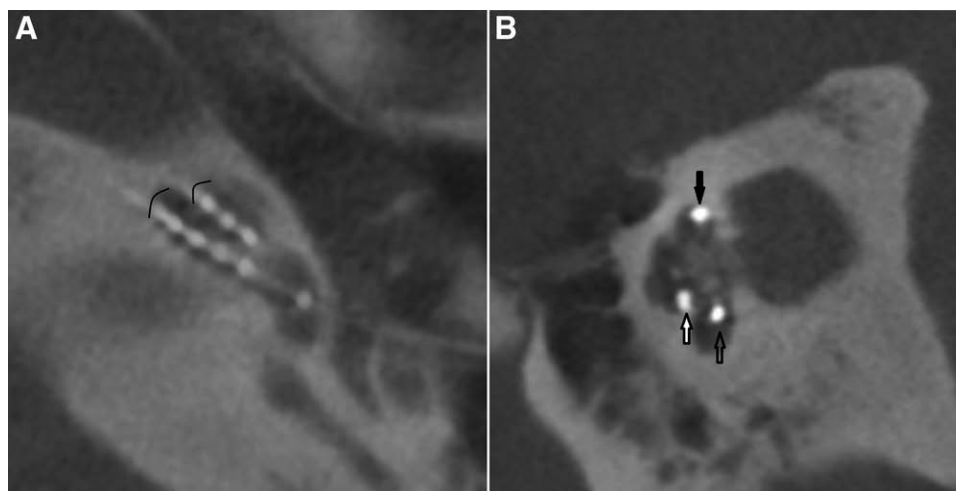


Fig. 4. A, Axial CBCT image of the Slim-J electrode array. Note the array is located within the scala tympani (posteriorly within the inferior segments of the middle and basal turns as indicated by the black arcs). B, Oblique sagittal reformatted image in the mid modiolar axis. The electrode contacts are demonstrated within the inferior segment of the basal turn (open black arrow), the superior segment of the basal turn (filled black arrow), and the inferior segment of the middle turn (black arrow filled with white). CBCT indicates cone beam computed tomography.

assessed by converting the Pearson correlation coefficient into a *t*-statistic using the following formula:

$$t = \frac{r\sqrt{n-2}}{\sqrt{1-r^2}}$$

where *r* is the correlation coefficient and *n* is the sample size. The correlation *t*-statistic was then checked for significance against the *t*-table for a two-tailed distribution with degrees of freedom (df) = *n* - 2 and reported as a *p* value, evaluating whether or not the *r* value is significantly different from zero for the given sample size.

RESULTS

A total of 12 patients were recruited into the study and underwent intraoperative ECoChG recording. This included 10 unilaterally implanted adults and two bilaterally implanted children (*n* = 14 ears, female:male = 8:4). The mean age at the

time of implantation was 56 years (range = 2–82). The data from an additional three participants who only underwent postoperative ECoChG at audiology follow-up were also included in the postoperative PTA to ECoChG correlation data. The range of etiologies and duration of deafness for all cases are shown in Table 1. All patients were implanted with the Slim-J Ultra 3D array, and full insertion was achieved up to the blue marker in all ears. There were no surgical complications in any of the cases.

A CM was successfully recorded in 13 out of 14 ears (93%). The 0.5 kHz intraoperative CM and postinsertion electrode sweep traces for each participant along with their preoperative, postoperative, and ECoChG predicted audiograms are given in Figures in Supplemental Digital Content 1, <http://links.lww.com/EANDH/A771>.

CBCT was performed for 12 out of 14 ears (86%), as one bilaterally implanted child was too young to comply with an awake scan. Full insertion of all active electrode contacts was confirmed in every case, with a mean angular insertion depth of

TABLE 1. Study participant demographic information, hearing loss etiology, testing status, and CI array code for Figure 10 and Supplemental Digital Content 1, <http://links.lww.com/EANDH/A771>

Age	Gender	Etiology	Intraoperative ECoChG	Postoperative CBCT	Electrode
4	F	Childhood acquired progressive SNHL unknown cause	Y & Y	Y & Y	1(R) & 2(L)
77	F	Adulthood acquired progressive SNHL unknown cause	Y	Y	3
74	F	Adulthood acquired progressive SNHL unknown cause	Y	Y	4
76	F	Adulthood acquired progressive SNHL unknown cause	Y	Y	5
2	M	Congenital profound—LVAS	Y & Y	N & N	6(L) & 7(R)
69	M	Adulthood acquired progressive SNHL and chronic otitis externa	Y	Y	8
81	F	Adulthood acquired progressive SNHL unknown cause	Y	Y	9
58	F	Adulthood acquired progressive SNHL unknown cause	Y	Y	10
81	M	Adulthood acquired progressive SNHL unknown cause	Y	Y	11
50	M	Adulthood acquired progressive SNHL unknown cause	Y	Y	12
32	F	Childhood acquired progressive SNHL unknown cause	Y	Y	13
64	F	Childhood acquired progressive SNHL unknown cause	Y	Y	14
68	M	Adulthood acquired progressive SNHL unknown cause	N	N/A	15
27	M	Congenital profound—LVAS	N	N/A	16
69	M	Adulthood acquired progressive SNHL unknown cause	N	N/A	17

TABLE 2. Distances in mm of each electrode contact from absolute tip of the Advanced Bionics Slim-J electrode array

Electrode	Distance from tip (mm)
1st (most apical)	0.5
2 nd	1.8
3 rd	3.1
4 th	4.4
5 th	5.7
6 th	7
7 th	8.3
8 th	9.6
9 th	10.9
10 th	12.3
11 th	13.5
12 th	14.8
13 th	16.1
14 th	17.4
15 th	18.7
16th (most basal)	20
Blue marker/Ref	23

431° (median=420, range=345–510). The electrode array was found to be located entirely within the scala tympani compartment in every ear that had postoperative imaging.

Figure 6 illustrates correlation between the measured and the ECoHG predicted postoperative PTA thresholds at 4 key frequencies (0.25, 0.5, 1, and 2 kHz) measured at the same time point postoperatively, using the scatter plot method described by Koka et al. 2017. Figure 7 plots this same data to show the distribution of dB HL error between measured and predicted postoperative thresholds for each frequency (0.25 kHz: -2.4 dB HL ± 13.4 SD, 0.5 kHz: 6.6 dB HL ± 11.5 SD, 1 kHz: 10.1 dB HL ± 8.1 SD, 2 kHz: 17 dB HL ± 8.9 SD).

During data collection, it was noted that the predicted behavioral thresholds for 0.25 and 0.5 kHz were considerably underestimated in the two cases where the newer plastic dome was used to deliver the sound stimulus. Further investigation revealed that there was significant loss of stimulus intensity at 0.25 (-11 dB SPL) and 0.5 kHz (-4 dB SPL), when using the plastic dome compared with the Etymotics 3A foam tip. Due to the concern with the stimulus intensity, the 0.25 and 0.5 kHz postoperative responses obtained with the plastic dome from these two patients were excluded from the final analysis. The use of the plastic dome was subsequently abandoned and the study reverted to the use of the foam tip. As this technical concern did not affect the higher stimulus frequencies (1 and 2 kHz), or the pattern and location of response on CBCT correlation, the data from these two patients were retained for the rest of the analysis.

With these data points excluded (plotted in red, Figs. 6 and 7), the 2 SD range (within which we would expect to find 95% of the population assuming a normal distribution) for the frequencies which would potentially be used for the acoustic amplification in an EAS device (0.25, 0.5, and 1 kHz) was ± 24 dB HL (solid lines Fig. 6). The dotted lines in Figure 6 represent the theoretical 2 SD range, which would be required for ECoHG predicted thresholds to be confidently used in lieu of behavioral responses with no significant detriment in accuracy. Of note, currently only 50% of these responses were within this theoretical 10 dB HL 2 SD range.

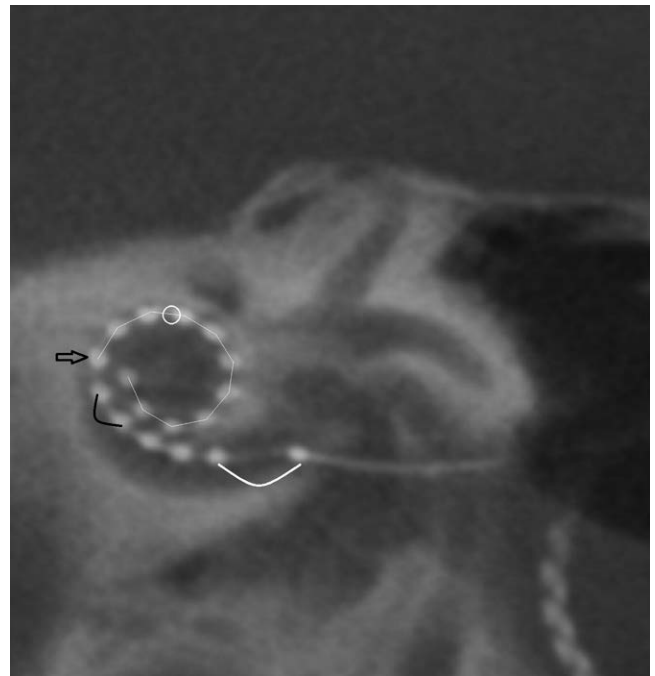


Fig. 5. Double oblique coronal reformatted image through the basal turn with a 2 mm average slab reconstruction designed to demonstrate the entire electrode array. A CM event was detected when electrode 11 passed through the round window. The final position of electrode 11 is indicated by the open black arrow. The intra-cochlear portion of the electrode array at the time of the CM event is delineated with a white line. The estimated location of the apical electrode at the time of the CM event is indicated by the white circle (as determined by counting the appropriate number of interspace gaps along the course of the electrode array at its final position). The black arc indicates the 1.3 mm inter-contact gap and the white arc indicates the 3 mm gap between the reference electrode and the most basal electrode contact (16), both of which are required to calculate the position of the apical electrode at the time of the CM event. CM indicates cochlear microphonic.

The hearing preservation outcomes at activation using the Skarzynski formula (Skarzynski et al. 2013) were as follows: 25% full preservation, 50% partial preservation, 8.3% minimal preservation, and 16.7% no preservation. Although the sample numbers were too small for statistical analysis, using the modified classification system as described earlier it was observed that only 7 out of 13 successful ECoHG recordings correctly predicted the hearing preservation outcome. In 5 out of the 6 incorrect predictions, the CM trace had predicted hearing preservation, but by the time of device activation, the residual hearing had deteriorated. In the remaining one case where no recordable CM response was obtained, there was partial preservation of residual hearing.

Using the method described of estimating the position of the apical electrode contact within the cochlea, expressed as angular depth based on the records of each electrode contact passing through the RW and the postoperative CBCT, significant correlation was found between intraoperative and postinsertion CM amplitudes at the two distinct CM event markers (maximum CM amplitude = 29° mean absolute error, $r=0.77$, $p=0.006$; $>10\%$ of maximum CM amplitude = 52° mean absolute error, $r=0.85$, $p=0.002$). Figure 9 illustrates this correlation on a schematic cochlea for the $>10\%$ peak CM amplitude data.

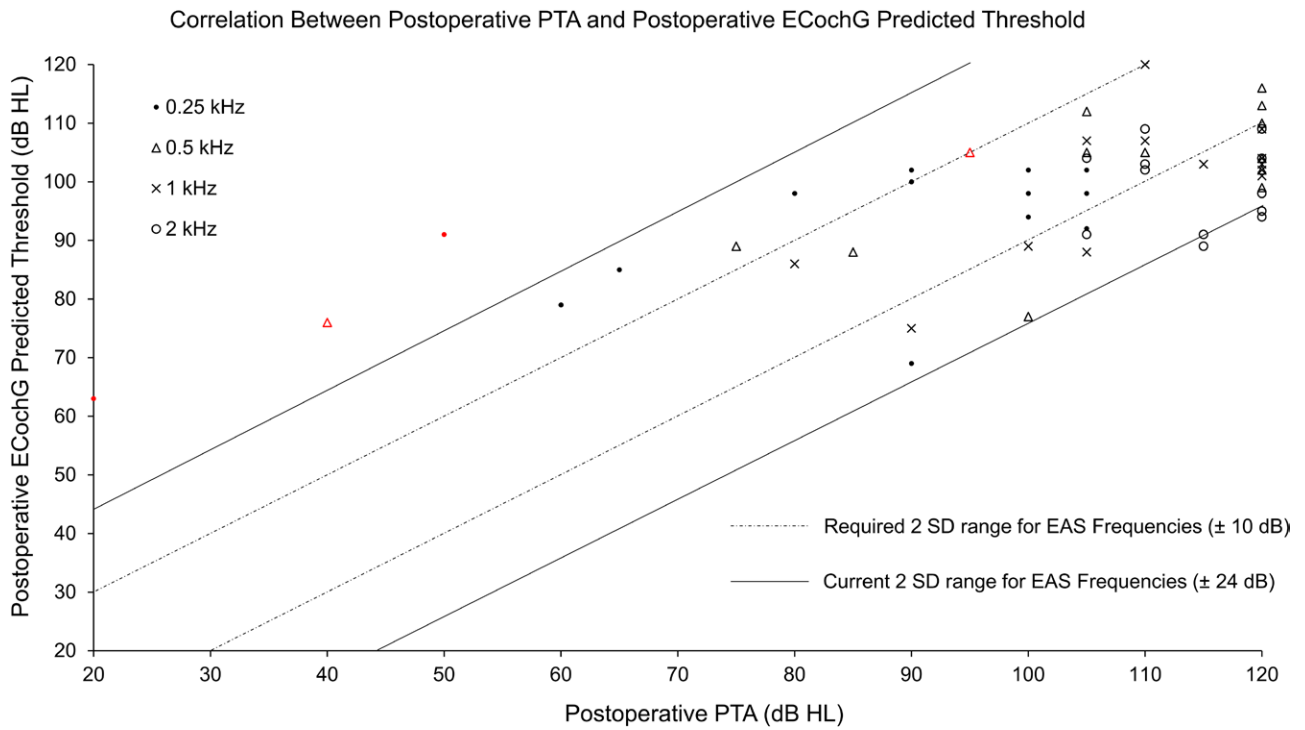


Fig. 6. Correlation of postoperative PTA threshold and postoperative ECoChG predicted hearing threshold at 4 key frequencies (0.25, 0.5, 1, and 2 kHz). Overlaid are the current 2 SD range (solid lines) and the 2 SD range that would be required to confidently fit EAS systems using ECoChG predictions (dotted lines). PTA indicates pure tone audiometry.

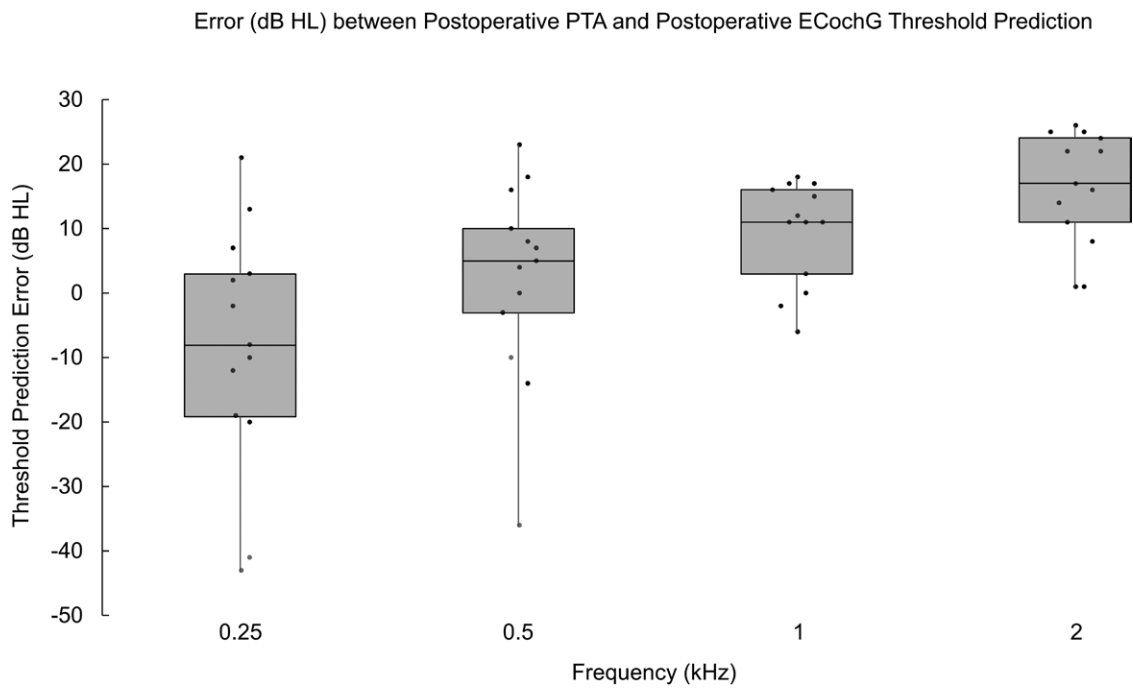


Fig. 7. Error in dB HL from the 6 weeks to 3 months postoperative PTA threshold to the ECoChG predicted hearing thresholds at 4 key frequencies (0.25, 0.5, 1, and 2 kHz). PTA indicates pure tone audiometry.

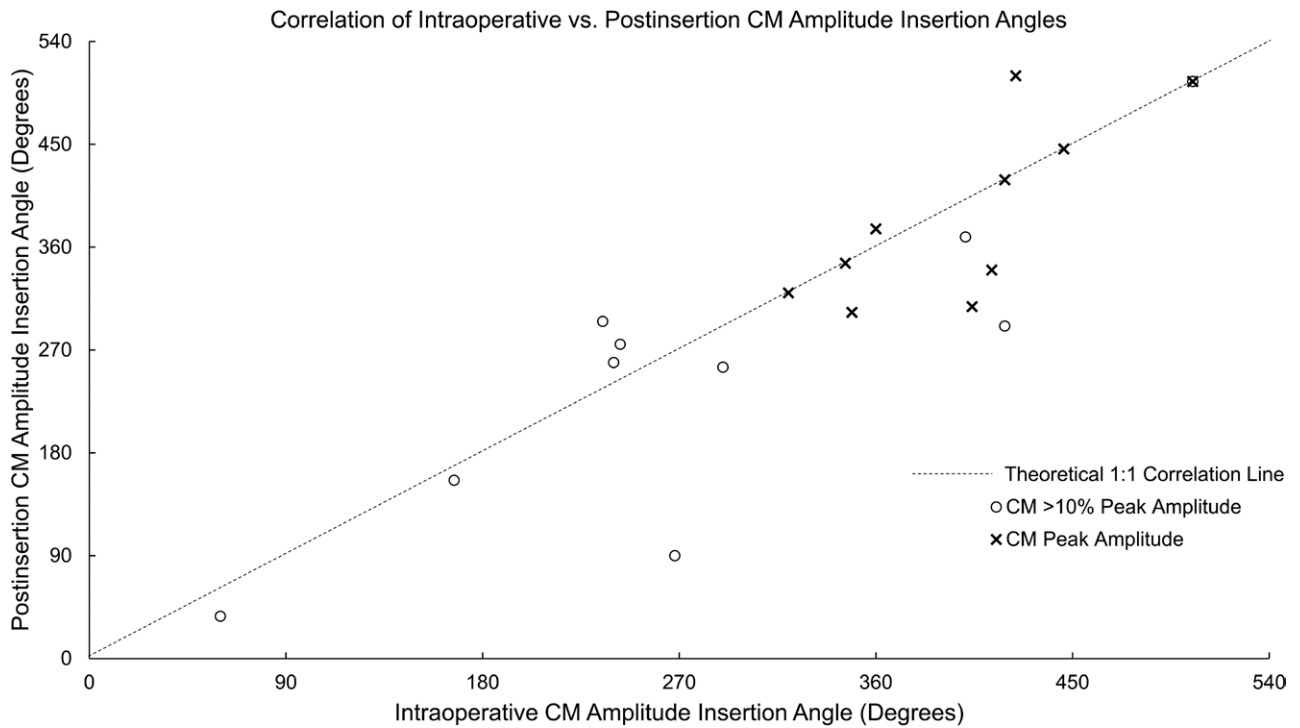
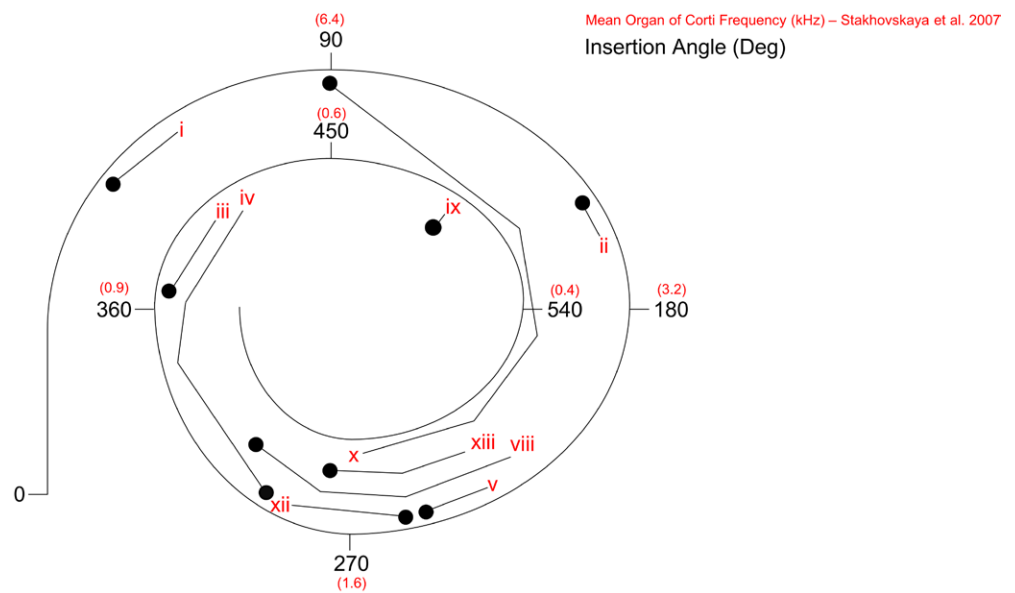


Fig. 8. Correlation of the insertion angles where the intraoperative and postinsertion cochlear microphonic peak amplitudes were reached (crosses); and correlation of the insertion angles where >10% of the intraoperative and postinsertion cochlear microphonic peak amplitudes were reached (circles). The dotted line represents a theoretical 1:1 insertion angle correlation.



- i Insertion angle where intraoperative CM amplitude exceeded 10% of max, numeral corresponding to electrode number in Table 1
- Insertion angle where postinsertion CM amplitude exceeded 10% of max

Fig. 9. Illustration on a schematic cochlea of the insertion angles where the intraoperative and postinsertion CM recordings reached >10% of peak amplitude. Roman numeral points correspond to electrode numbers in Table 1. CM indicates cochlear microphonic.

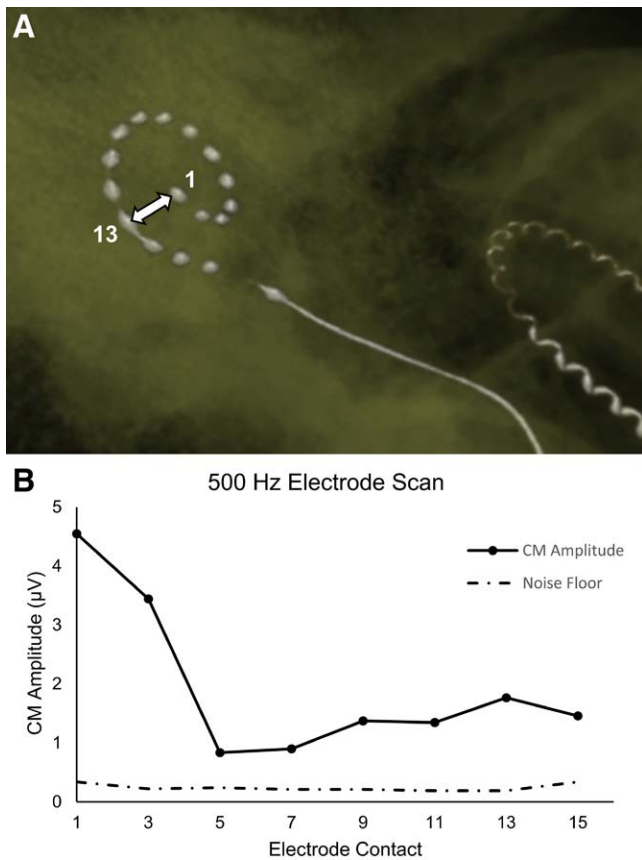


Fig. 10. A, CBCT showing electrode contact 1 being located in the middle turn of the cochlea directly above and in close absolute proximity to electrode contact 13 in the basal turn. B, CM amplitudes during a 0.5 kHz electrode sweep immediately postinsertion. The CM amplitude peaks at electrode 1 before falling to the noise floor at electrode 5. A secondary broader lower amplitude peak is centered on electrode 13. CBCT indicates cone beam computed tomography; CM, cochlear microphonic.

The 0.5 kHz CM amplitude was observed to peak towards the apex in all cases, both intraoperatively (mean 400°, median 413°, range 320°–505°) and postinsertion (mean 390°, median 376°, range 303°–510°). For the two patients, in whom significant postinsertion “electrode sweep” CMs were observed using 0.75–2 kHz stimuli, these were tonotopically distributed with peak responses moving to more basal electrodes for higher stimulus frequencies (Supplemental Digital Content 1, <http://links.lww.com/EANDH/A771> for their multifrequency “electrode sweep” responses, ears 5 and 10).

In the process of correlating each individual’s ECoChG recording to their CBCT, a potential example of cross-turn ECoChG recording was identified. In this case, the electrode contact 1, from which the peak CM amplitude was recorded during the 0.5 kHz postinsertion sweep, was found on CBCT to be located spatially adjacent to the much more basal electrode contact 13, which was the apex of a lower amplitude secondary CM peak (Fig. 10A, B). However, this combination of findings was not observed in the rest of the study cohort and it was therefore not possible to ascertain whether or not it was a true phenomenon.

Finally, an individual cochlear map of CM responses at electrode contact positions was created for each participant. A traffic light system was implemented to minimize the effect of confounding off-frequency and far-field hair cell stimulation

(Fig. 11). The intraoperative 0.5 kHz CM data and the electrode sweeps taken postinsertion at higher frequencies were used in combination to identify regions with a clear CM (electrode contacts with green markers). Electrode contacts in a region with no CM were denoted in red. Those in yellow were situated in areas of the cochlea where a low-amplitude CM was detected with a 0.5 kHz stimulus (<10% eventual max amplitude), but there was no CM observed with higher stimulus frequencies, in other words, presumed to be far-field CM detection.

DISCUSSION

Intraoperative Hearing Preservation

Although it was not one of the primary aims of this particular feasibility study, our center have been collecting data on ECoChG and hearing preservation. Our observation to date suggests a poor correlation between the intraoperative CM traces and hearing preservation at device activation. In 5 out of the 6 “incorrect” ECoChG hearing preservation predictions, the intraoperative CM amplitude was maintained throughout but there was partial or total hearing loss by switch-on. This postoperative deterioration in hearing thresholds, presumably caused by inflammatory processes related to surgically manipulating the cochlea, may be one of the limiting factors in the ability of CM to predict successful hearing preservation. In the other case of no recordable CM but partial hearing preservation, the residual hair cell population may have been insufficient to generate a recordable intraoperative CM (preoperative PTA threshold at 500 Hz = 90 dB HL). A lack of correlation between intraoperative ECoChG thresholds and postoperative behavioral thresholds has been previously observed (O’Connell et al. 2017).

One possible explanation for the poor correlation between CM recordings and hearing preservation in our cohort is the fact that all study participants had relatively poor hearing preoperatively. There is some evidence that it is more difficult to preserve residual hearing in this population (Wanna et al. 2018). There is also ongoing work to improve the robustness of the measure for the purpose of hearing preservation, for example incorporating the change in phase of the CM response, factoring in a gradual drop in amplitude toward the end of the insertion for a 0.5 kHz stimulus and making recordings from multiple frequencies simultaneously (Saoji et al. 2019). Nevertheless, it remains to be seen whether it is feasible to act on that feedback, or if damage has already been done by the time a change in amplitude is seen. Previous work on animal models has shown irreversible drops in CM amplitude to be associated with visible basilar membrane trauma, while in some cases of reversible change in CM amplitude no such damage was seen histologically (DeMason et al. 2012), suggesting that acting on CM amplitude feedback in time may be technically possible.

Correlation With Audiometry

Our findings with regard to audiometric correlation were slightly poorer than those reported in other studies (Koka et al. 2017; Attias et al. 2020), but it is acknowledged that the stimulus level was not calibrated postoperatively for each patient in our study. Nonetheless, at 0.5 and 1 kHz, more than 80% of predicted thresholds were within 15 dB HL and more than 95% within 20 dB HL (Figs. 6 and 7). If the test/retest error of PTA were to be used as the gold standard for correlation,

Patient specific electrode array maps of CM sensitive cochlear regions

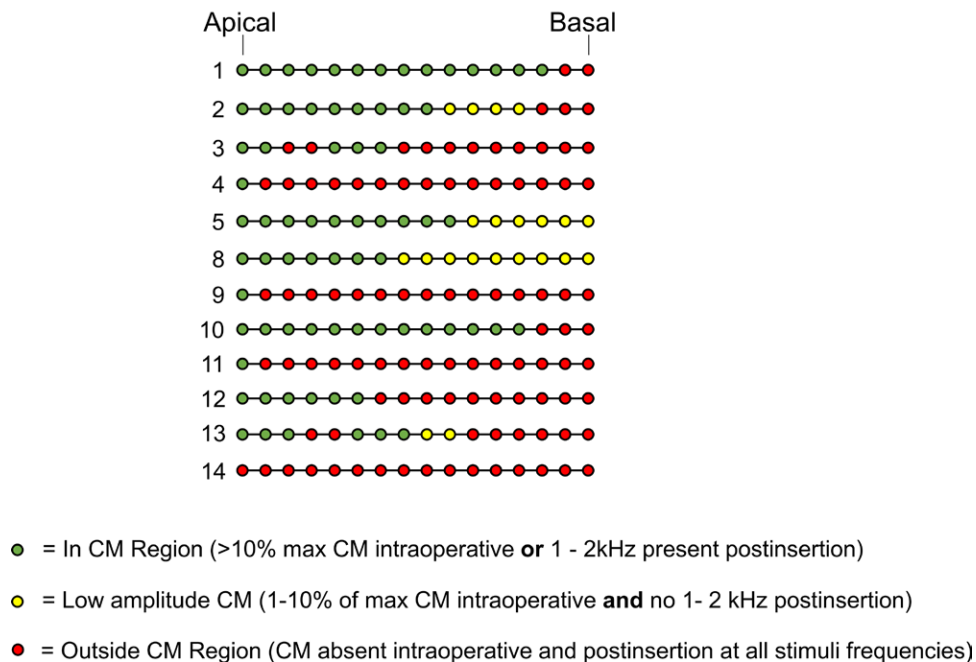


Fig. 11. Patient specific electrode array maps showing electrodes within regions with a cochlear microphonic detected (green), no cochlear microphonic detected (red), or a low-amplitude (<10% peak amplitude) intraoperative cochlear microphonic in response to 0.5 kHz when no higher frequency postinsertion cochlear microphonic was present (yellow). The rationale for this traffic light system is that the “yellow” responses are more likely to be a “far-field” detection of the 0.5 kHz microphonic and thus not representative of functional hair cells at that position in the cochlea.

the ECochG predicted thresholds would need be within 5 dB at any frequency for almost all cases (>95%) in adults, and within 10 dB for infants due to the additional challenges associated with testing this age group. Therefore, further improvement from the currently observed 24 dB HL 2 SD range is required before ECochG predicted thresholds could be used with confidence to fit EAS CI devices. On the other hand, it should also be acknowledged that there is likely to be a limit to how well CM responses can be correlated to behavioral responses. For example, it has been posited that in cochleae with significant hearing loss it may be relatively common for there to be populations of functional hair cells, which are disconnected from spiral ganglion neurons (Fontenot et al. 2019).

In our study cohort, the two mid frequencies (0.5 and 1 kHz) appeared to be more accurate than those on either end of the frequency range. This may have been exacerbated by a change in the type of insert tip used in the ear canal as a result of moving from the “Black Box” to the “AIM” device for recording. It is widely recognized that it is very difficult to retain low-frequency stimulation in an ear canal with anything but the most occlusive of moulds (Dillon 1991). Preliminary real ear measurements showed that, even under optimal conditions, the gain with the new tip was reduced compared with the older foam tip by 15 dB at 0.125, 10 dB at 0.25, and 5 dB at 0.5 kHz (See Figure in Supplemental Digital Content 2, <http://links.lww.com/EANDH/A772>). Additionally, the gain was reduced further if the dome was not optimally positioned, which did not seem to affect the foam tip. This reduced stimulus level would explain why the threshold calculation algorithm used was underestimating

residual hearing at these frequencies, with the sound pressure level at the tympanic membrane being lower than assumed by the algorithm; as discussed previously, it was not possible to calibrate intraoperatively to compensate for this. Both patients for whom the new tip was used postoperatively showed large deviations in error to the other data in the low frequencies (red markers Figs. 6 and 7).

For 2 kHz, it is worth noting that our real ear measurements (Figure in Supplemental Digital Content 2, <http://links.lww.com/EANDH/A772>) showed the dB SPL at the ear drum for this stimulus frequency was approximately 10 dB higher than anticipated, suggesting that the stimulus delivery was not accounting for the real ear resonance, thus making the 2 kHz stimuli objectively louder than the other frequencies at which the natural ear canal resonance has much more limited effect. This error would likely vary on a patient-to-patient basis, but it might explain some of the observed overestimation in predicted hearing thresholds at this frequency and emphasizes the importance of stimulus calibration as an avenue for improving ECochG to PTA correlation. Additionally, the microphonic response for 2 kHz is being generated at a more basal position in the cochlea compared with the apical recording electrode contact (Greenwood 1990), leaving room for the introduction of additional error in the formula used to predict behavioral thresholds.

One strategy that could rectify this issue would be to record from a more basal electrode closer to where the 2 kHz CM is likely to be generated. The validity of this was difficult to test comprehensively in our cohort, since, in most cases, the

overestimation stemmed from a recordable CM at 2 kHz but with an absent PTA response at this frequency. Thus, although these responses disappeared when recording from a more basal electrode and at a slightly lower stimulus intensity (100 dB SPL), it is difficult to ascertain whether this was due to genuinely improved correlation with PTA or general ineffectiveness of this method in recording the CM; this approach will therefore need to be trialed in patients who have some residual hearing at 2 kHz.

Finally, the current standard algorithm for hearing prediction takes the amplitude of the CM generated by up to 110 dB SPL and performs a single point linear regression to estimate the loudness required to generate a threshold CM. A more accurate method would likely be to record the CM amplitude at several loudness levels (i.e., 110, 100, and 90 dB SPL) to plot a line of best fit to threshold (Krüger et al. 2020). This approach and its potential to improve the audiometric correlation is currently under investigation at our center. In general, CM measurements from CI in situ appear to be a promising method for accurately estimating residual hearing at device activation. With these proposed developments in methodology, predictive accuracy of ≤ 10 dB HL per frequency in more than 95% of cases could be achievable in the future, making it a useful clinical tool for fitting EAS devices.

Test-retest Correlation of Cochlear Microphonic With Cochlear Position Using CBCT

Since there is currently no imaging technique that can visualize the electrode array moving through the cochlea in real time with sufficient resolution, we have developed a novel approach to estimate the position of the apical electrode contact, based on each electrode contact passing through the RW and postoperative CBCT. Although we are confident, from the quality of CBCT at our center and the experience we have with this imaging modality, that we can assess the angular depth of insertion to the nearest 5°, our approach has one confound of assuming that the final position of the electrode array seen on postoperative CBCT is identical to its trajectory during insertion. It is hoped that it will be possible in the future to develop a method to visualize of the electrode array real time or, at least, to “track” its route more accurately; however, the current approach has already provided us with an ability to check for correlation with electrode function.

The correlation of the CM between the intraoperative and postinsertion measurements appeared to be robust. In only one case (See Figs. 8 and 9) was there significant disagreement between the two on the location where the CM began to increase in amplitude. It was noted, however, that for this participant the CM itself was of low amplitude throughout (See Figure in Supplemental Digital Content 1, <http://links.lww.com/EANDH/A771>), which may explain the discrepancy.

In several cases the intraoperative CM reached peak amplitude before the end of the insertion then diminishing slightly. In cases where this pattern occurred intraoperatively we also observed in the 0.5 kHz postinsertion electrode sweeps that electrode contact 3 had a higher CM amplitude than electrode contact 1. This reproducibility in the site of the maximal CM amplitude between intraoperative and postinsertion measurements appears to suggest that the 0.5 kHz CM peak occurring before full insertion intraoperatively and then decreasing is not due to the array somehow impinging on the basilar membrane

or otherwise permanently altering its movement; if this were the case we would not expect the postinsertion recordings to also show a similar pattern of peak CM amplitude once the electrode had been moved further on. A previous study (Riggs et al. 2019) similarly observed that the apical electrode CM amplitude at full insertion was similar to the amplitude at the first blue marker (between electrodes 5 and 6), which could also suggest that the 500 Hz CM amplitude was peaking somewhere in between these two points.

There are two other plausible hypotheses for these observed decreases. The most intuitive is that the apical electrode contact has gone past the tonotopic site of signal generation for 0.5 kHz. Previous work modeling and mapping the organ of Corti (Greenwood 1990; Stakhovskaya et al. 2007) suggests this should be unlikely for an electrode with a 23 mm insertion depth. However, it should be borne in mind that these studies used a predictive model and studied a limited sample size respectively, neither of which provide certainty that they have captured the variance of the population fully. Furthermore, what effect, if any, profound hearing losses of various etiologies and their associated loss of functional and supporting cells in the cochlea might have on the basilar membrane tuning curve is not known.

Another, and possibly a more likely, explanation which has also recently been proposed by Giardina et al. 2019 is that this decrease is an interference effect of more basal hair cells being stimulated and detected out of phase to the actual 0.5 kHz signal generator site, resulting in a destructive interference pattern. These artifacts, which create characteristic double amplitude CM peaks centered close to a phase shift in the response, have previously been observed in animal studies (Kohllöffel 1970). In these animal studies, a mathematical model using realistic estimates for the tuning curve and phase functions of the guinea pig basilar membrane seemed able to correctly predict the morphology of these CM patterns. Our regular observation of these characteristic double peak responses would support this hypothesis, as would our failure to observe such patterns in any cases where residual hearing, and thus likely basal hair cells capable of being stimulated out of phase, was absent at all higher frequencies (>0.5 kHz). Regardless of the exact underlying mechanism, this uncertainty as to why the CM may decrease at certain points of the recording needs to be understood before we can use the traces to guide surgical practice with confidence.

Cochlear Microphonic Maps

It is well established that maintenance of the hearing pathway by appropriate stimulation prevents, or at least slows, spiral ganglion atrophic degeneration (Leake et al. 1999). It seems reasonable, therefore, to hypothesize that a region of the cochlea which has functioning hair cells and produces a measurable CM is more likely to have coincident functioning spiral ganglion neurons in the vicinity. Supporting this notion, Fontenot et al. 2019 recently demonstrated correlation between the summed amplitude of CM responses recorded from the RW across several frequencies prior to electrode insertion and CI speech perception outcomes. There is also some evidence that CIs function better with a more robust neural population in the vicinity (Seyyedi et al. 2014). In view of these findings, it would seem a logical next step to explore whether electrode contacts that lie within regions of the cochlea from which a CM was

recorded have more favorable psychoacoustic properties for the encoding of sound information.

In order to be able to test this hypothesis, our first step has been to create individual maps of each participant's CM correlated to their cochlea and determine which contacts along the electrode array are within a region where a microphonic was detected using a traffic light system (Fig. 10). Using this system it was possible to differentiate between contacts at which we were relatively confident a near field CM was detected (green) and those we were not (yellow). For contacts marked yellow assumption was made that the low level 0.5 kHz CM was being detected in a far-field manner from the characteristically sensitive region for this frequency. This is because, if it were instead caused by off-frequency stimulation of the basal hair cells in the region of these yellow marked contacts, it should have been possible to record CMs in response to higher frequency stimuli from them.

Characterizing Tonotopic Cochlea Microphonic Responses

As discussed previously, there is currently much that is not completely understood regarding the importance of the phase of the CM response and the change of its phase over time. In addition, the relationship between moderate changes in CM amplitude and the true site of signal generation in the cochlea has yet to be satisfactorily elucidated. Our study has observed in two cases gross tonotopicity of the microphonic responses when using a range of stimulus frequencies, which, in addition to observation of suspected cross-turn effects, is strongly suggestive of localized CM detection. Being able to determine more reliably exactly where the signal generator lies based on observed CM amplitude patterns and/or phase changes might enable us to utilize this tonotopic information to improve place pitch correlation, or predict, and thus help alleviate, inter-electrode interference.

Limitations of the Study

The authors acknowledge that our study has a number of limitations. Firstly, the sample size is relatively small; however, due to the strength of the correlation (effect size), a post hoc power analysis suggested the statistical significance analysis performed was suitably powered. Secondly, as was previously mentioned regarding CBCT correlation, the final position of the electrode observed on postoperative imaging may not exactly match the path the electrode has taken during insertion. Thirdly, there are a number of areas in which our protocol for ECoChG audiometric threshold estimation could be improved, such as calibration of the stimuli using a real ear measurement, using several steps in intensity to calculate the linear regression, and recording CM amplitudes from electrodes likely to be closest to the characteristic frequency location for the stimulus frequency being used.

Finally, from a theoretical standpoint the greatest limitation continues to be the incomplete understanding of the ECoChG signal itself when recorded from a moving electrode within the cochlea, in terms of which component is the most robust, reliable, repeatable, and clinically relevant. For example, it is not yet clear if interference patterns are a significant confounding factor, if the CM phase information can be reliably used, or how changes in CM amplitude relate

to hearing preservation or cochlear function. Furthermore, it is possible that technical advances in ECoChG recording and signal processing may show other components, such as the ANN, to be more useful in the context of CI surgery and rehabilitation.

CONCLUSION

Here we have described a novel method to demonstrate for the first time the reproducibility of the CM responses recorded from a CI electrode during insertion. By correlating the CM amplitude with each participant's postoperative CBCT, we have also been able to create individualized maps of CM responses, categorizing their cochleae into acoustically responsive and unresponsive regions. We now plan to conduct psychoacoustic testing on these patients, namely an intensity difference limen test, in order to establish whether or not the electrode contacts within these acoustically sensitive regions demonstrate improved loudness discrimination, which could have implications for optimal electrode mapping and placement.

ACKNOWLEDGMENTS

A.J.S. designed the study, collected and analyzed the data, and prepared the article. S.C. designed the study, collected and analyzed the data, and contributed to article preparation. D.J. designed the study, collected the data, and contributed to article preparation. T.N. contributed to data analysis and article preparation. P.B. provided technical advice and contributed to data analysis and article preparation. I.P. designed the study, collected and analyzed the data, and prepared the article. All authors provided critical revision of the article and gave final approval of the article.

Address for correspondence: Dan Jiang, St. Thomas' Hearing Implant Centre, Guy's and St. Thomas' NHS Foundation Trust, London SE1 7EH, United Kingdom. E-mail: dan.jiang@kcl.ac.uk

Advanced Bionics provided the "Black Box 2" and "AIM tablet" electrocochleography recording devices on a loan basis for the purposes of this study. Dr. Patrick Boyle is used by Advanced Bionics. There are no other conflicts of interest or sponsorship to declare.

Data Sharing Statement: Researchers interested in obtaining access to the study protocol and anonymized datasets for future research should submit a one-page research proposal to St. Thomas' Hearing Implant Centre Data Access Committee (gst-tr.hearingimplants@nhs.net) stating the research question, importance, and methods, together with an appendix listing the detail of data points required. The Access Committee will consider the research question, together with any thematic overlap with existing projects, and make a decision. A registry of all applications will be maintained for audit. The terms of sharing the anonymised datasets will be subject to separate Data Sharing Agreement.

The authors confirm full editorial control of the manuscript.

Received June 12, 2020; accepted December 1, 2020; published online ahead of print April 2, 2021.

REFERENCES

- Attias, J., Ulanovski, D., Hilly, O., Greenstein, T., Sokolov, M., HabibAllah, S., Mormer, H., Raveh, E. (2020). Postoperative intracochlear electrocochleography in pediatric cochlear implant recipients: Association to audiometric thresholds and auditory performance. *Ear Hear*, *41*, 1135–1143.
- Bester, C. W., Campbell, L., Dragovic, A., Collins, A., O'Leary, S. J. (2017). Characterizing electrocochleography in cochlear implant recipients with residual low-frequency hearing. *Front Neurosci*, *11*, 141.
- Campbell, L., Kaicer, A., Sly, D., Iseli, C., Wei, B., Briggs, R., O'Leary, S. (2016). Intraoperative real-time cochlear response telemetry

- predicts hearing preservation in cochlear implantation. *Otol Neurotol*, 37, 332–338.
- Choudhury, B., Fitzpatrick, D. C., Buchman, C. A., Wei, B. P., Dillon, M. T., He, S., Adunka, O. F. (2012). Intraoperative round window recordings to acoustic stimuli from cochlear implant patients. *Otol Neurotol*, 33, 1507–1515.
- Conlon, B. J., & Gibson, W. P. (2000). Electrocochleography in the diagnosis of Meniere's disease. *Acta Otolaryngol*, 120, 480–483.
- Dalbert, A., Pfiffner, F., Rössli, C., Thoele, K., Sim, J. H., Gerig, R., Huber, A. M. (2015). Extra- and intracochlear electrocochleography in cochlear implant recipients. *Audiol Neurotol*, 20, 339–348.
- DeMason, C., Choudhury, B., Ahmad, F., Fitzpatrick, D. C., Wang, J., Buchman, C. A., Adunka, O. F. (2012). Electrophysiological properties of cochlear implantation in the gerbil using a flexible array. *Ear Hear*, 33, 534–542.
- Dillon, H. (1991). Allowing for real ear venting effects when selecting the coupler gain of hearing aids. *Ear Hear*, 12, 406–416.
- Dodson, H. C., & Mohiuddin, A. (2000). Response of spiral ganglion neurons to cochlear hair cell destruction in the guinea pig. *J Neurocytol*, 29, 525–537.
- Eggermont, J. J. (2019). Cochlea and auditory nerve. *Handb Clin Neurol*, 160, 437–449.
- Eppsteiner, R. W., Shearer, A. E., Hildebrand, M. S., Deluca, A. P., Ji, H., Dunn, C. C., Black-Ziegelbein, E. A., Casavant, T. L., Braun, T. A., Scheetz, T. E., Scherer, S. E., Hansen, M. R., Gantz, B. J., Smith, R. J. (2012). Prediction of cochlear implant performance by genetic mutation: The spiral ganglion hypothesis. *Hear Res*, 292, 51–58.
- Fitzpatrick, D. C., Campbell, A. P., Campbell, A. T., Choudhury, B., Dillon, M. T., Dillon, M. P., Forgues, M., Buchman, C. A., Adunka, O. F. (2014). Round window electrocochleography just before cochlear implantation: Relationship to word recognition outcomes in adults. *Otol Neurotol*, 35, 64–71.
- Fontenot, T. E., Giardina, C. K., Dillon, M., Rooth, M. A., Teagle, H. F., Park, L. R., Brown, K. D., Adunka, O. F., Buchman, C. A., Pillsbury, H. C., Fitzpatrick, D. C. (2019). Residual cochlear function in adults and children receiving cochlear implants: Correlations with speech perception outcomes. *Ear Hear*, 40, 577–591.
- Giardina, C. K., Brown, K. D., Adunka, O. F., Buchman, C. A., Hutson, K. A., Pillsbury, H. C., Fitzpatrick, D. C. (2019). Intracochlear electrocochleography: Response patterns during cochlear implantation and hearing preservation. *Ear Hear*, 40, 833–848.
- Greenwood, D. D. (1990). A cochlear frequency-position function for several species—29 years later. *J Acoust Soc Am*, 87, 2592–2605.
- Harris, M. S., Riggs, W. J., Giardina, C. K., O'Connell, B. P., Holder, J. T., Dwyer, R. T., Koka, K., Labadie, R. F., Fitzpatrick, D. C., Adunka, O. F. (2017). Patterns seen during electrode insertion using intracochlear electrocochleography obtained directly through a cochlear implant. *Otol Neurotol*, 38, 1415–1420.
- Henry, K. R. (1995). Auditory nerve neurophonic recorded from the round window of the Mongolian gerbil. *Hear Res*, 90, 176–184.
- Kohllöffel, L. U. E. (1970). Longitudinal amplitude and phase distribution of the cochlear microphonic (guinea pig) and spatial filtering. *J Sound Vib*, 11, 325–334.
- Koka, K., Riggs, W. J., Dwyer, R., Holder, J. T., Noble, J. H., Dawant, B. M., Ortmann, A., Valenzuela, C. V., Mattingly, J. K., Harris, M. M., O'Connell, B. P., Litvak, L. M., Adunka, O. F., Buchman, C. A., Labadie, R. F. (2018). Intra-cochlear electrocochleography during cochlear implant electrode insertion is predictive of final scalar location. *Otol Neurotol*, 39, e654–e659.
- Koka, K., Saoji, A. A., Litvak, L. M. (2017). Electrocochleography in cochlear implant recipients with residual hearing: Comparison with audiometric thresholds. *Ear Hear*, 38, e161–e167.
- Krüger, B., Büchner, A., Lenarz, T., Nogueira, W. (2020). Amplitude growth of intracochlear electrocochleography in cochlear implant users with residual hearing. *J Acoust Soc Am*, 147, 1147.
- Laureano, A. N., McGrady, M. D., Campbell, K. C. (1995). Comparison of tympanic membrane-recorded electrocochleography and the auditory brainstem response in threshold determination. *Am J Otol*, 16, 209–215.
- Leake, P. A., Hradek, G. T., Snyder, R. L. (1999). Chronic electrical stimulation by a cochlear implant promotes survival of spiral ganglion neurons after neonatal deafness. *J Comp Neurol*, 412, 543–562.
- Nayagam, B. A., Muniak, M. A., Ryugo, D. K. (2011). The spiral ganglion: Connecting the peripheral and central auditory systems. *Hear Res*, 278, 2–20.
- O'Connell, B. P., Holder, J. T., Dwyer, R. T., Gifford, R. H., Noble, J. H., Bennett, M. L., Rivas, A., Wanna, G. B., Haynes, D. S., Labadie, R. F. (2017). Intra- and postoperative electrocochleography may be predictive of final electrode position and postoperative hearing preservation. *Front Neurosci*, 11, 291.
- O'Neil, J. N., Connelly, C. J., Limb, C. J., Ryugo, D. K. (2011). Synaptic morphology and the influence of auditory experience. *Hear Res*, 279, 118–130.
- Rance, G., Beer, D. E., Cone-Wesson, B., Shepherd, R. K., Dowell, R. C., King, A. M., Rickards, F. W., Clark, G. M. (1999). Clinical findings for a group of infants and young children with auditory neuropathy. *Ear Hear*, 20, 238–252.
- Riggs, W. J., Dwyer, R. T., Holder, J. T., Mattingly, J. K., Ortmann, A., Noble, J. H., Dawant, B. M., Valenzuela, C. V., O'Connell, B. P., Harris, M. S., Litvak, L. M., Koka, K., Buchman, C. A., Labadie, R. F., Adunka, O. F. (2019). Intracochlear electrocochleography: Influence of scalar position of the cochlear implant electrode on postinsertion results. *Otol Neurotol*, 40, e503–e510.
- Rutkove, S. B. (2007). Introduction to volume conduction. In A. S. Blum, & S. B. Rutkove (Eds.), *The Clinical Neurophysiology Primer* (p. 43). Humana Press.
- Santarelli, R., & Arslan, E. (2002). Electrocochleography in auditory neuropathy. *Hear Res*, 170, 32–47.
- Santarelli, R., Scimemi, P., Dal Monte, E., Arslan, E. (2006). Cochlear microphonic potential recorded by transtympanic electrocochleography in normally-hearing and hearing-impaired ears. *Acta Otorhinolaryngol Ital*, 26, 78–95.
- Saoji, A. A., Patel, N. S., Carlson, M. L., Neff, B. A., Koka, K., Tarigoppula, V. S. A., Driscoll, C. L. W. (2019). Multi-frequency electrocochleography measurements can be used to monitor and optimize electrode placement during cochlear implant surgery. *Otol Neurotol*, 40, 1287–1291.
- Seyyedi, M., Viana, L. M., Nadol, J. B. Jr. (2014). Within-subject comparison of word recognition and spiral ganglion cell count in bilateral cochlear implant recipients. *Otol Neurotol*, 35, 1446–1450.
- Skarzynski, H., Van de Heyning, P., Lorens, A., Mertens, G., et al. (2013). Towards a consensus on a hearing preservation classification system. *Acta Otolaryngol*, 133(suppl 564), 3–13.
- Snyder, R. L., & Schreiner, C. E. (1984). The auditory neurophonic: Basic properties. *Hear Res*, 15, 261–280.
- Stakhovskaya, O., Sridhar, D., Bonham, B. H., Leake, P. A. (2007). Frequency map for the human cochlear spiral ganglion: Implications for cochlear implants. *J Assoc Res Otolaryngol*, 8, 220–233.
- Terayama, Y., Kaneko, Y., Kawamoto, K., Sakai, N. (1977). Ultrastructural changes of the nerve elements following disruption of the organ of Corti. I. Nerve elements in the organ of Corti. *Acta Otolaryngol*, 83, 291–302.
- Tropitzsch, A., Dofek, S., Schneider, F., Gammerringer, P., Lodes, S., Müller, M., Löwenheim, H., Vona, B., Holderried, M. (2019). Outcome prediction in cochlear implant patients, a genotype-phenotype correlation. *Laryngorhinootologie*, 98(Suppl 02), 11463.
- Wanna, G. B., O'Connell, B. P., Francis, D. O., Gifford, R. H., Hunter, J. B., Holder, J. T., Bennett, M. L., Rivas, A., Labadie, R. F., Haynes, D. S. (2018). Predictive factors for short- and long-term hearing preservation in cochlear implantation with conventional-length electrodes. *Laryngoscope*, 128, 482–489.
- Webster, M., & Webster, D. B. (1981). Spiral ganglion neuron loss following organ of Corti loss: A quantitative study. *Brain Res*, 212, 17–30.